Functional and Structural Insights of the Zinc-Finger HIT protein family members Involved in Box C/D snoRNP Biogenesis

Benoit Bragantini, Decebal Tiotiu, Benjamin Rothé, Jean-Michel Saliou, Hélène Marty, Sarah Cianférani, Bruno Charpentier, Marc Quinternet, Xavier Manival

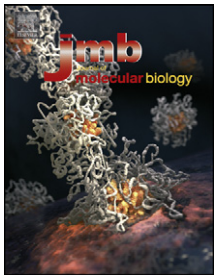

Functional and Structural Insights of the Zinc-Finger HIT protein family members Involved in Box C/D snoRNP Biogenesis

Benoit Bragantini [1,†], Decebal Tiotiu [1,†], Benjamin Rothé [1], Jean-Michel Saliou [3,4], Hélène Marty [1], Sarah Cianférani [3,4], Bruno Charpentier [1], Marc Quinternet [2] and Xavier Manival [1]

*1 - **Ingénierie Moléculaire et Physiopathologie Articulaire (IMoPA),** UMR 7365, CNRS Université de Lorraine, Biopôle, Campus Biologie-Santé, 9 Avenue de la Forêt de Haye, CS 50184, 54505 Vandœuvre-lès-Nancy, France*
*2 - **FR 3209,** CNRS-Université de Lorraine, Bioingénierie Moléculaire, Cellulaire et Thérapeutique, Biopôle, Campus Biologie-Santé, CS 50184, 54505 Vandœuvre-lès-Nancy Cedex, France*
*3 - **BioOrganic Mass Spectrometry Laboratory (LSMBO),** IPHC, Université de Strasbourg, 25 rue Becquerel, 67087 Strasbourg, France*
*4 - **IPHC,** UMR 7178, CNRS, 67087 Strasbourg, France*

***Correspondence to Marc Quinternet and Xavier Manival:** marc.quinternet@univ-lorraine.fr; xavier.manival@univ-lorraine.fr*
http://dx.doi.org/10.1016/j.jmb.2016.04.028
Edited by Mingjie Zhang

Abstract

Zf–HIT family members share the zf–HIT domain (ZHD), which is characterized by a fold in "treble-clef" through interleaved CCCC and CCHC ZnF motifs that both bind a zinc atom. Six proteins containing ZHD are present in human and three in yeast proteome, all belonging to multimodular RNA/protein complexes involved in gene regulation, chromatin remodeling, and snoRNP assembly. An interesting characteristic of the cellular complexes that ensure these functions is the presence of the RuvBL1/2/Rvb1/2 ATPases closely linked with zf–HIT proteins. Human ZNHIT6/BCD1 and its counterpart in yeast Bcd1p were previously characterized as assembly factors of the box C/D snoRNPs. Our data reveal that the ZHD of Bcd1p is necessary but not sufficient for yeast growth and that the motif has no direct RNA-binding capacity but helps Bcd1p maintain the box C/D snoRNAs level in steady state. However, we demonstrated that Bcd1p interacts nonspecifically with RNAs depending on their length. Interestingly, the ZHD of Bcd1p is functionally interchangeable with that of Hit1p, another box C/D snoRNP assembly factor belonging to the zf–HIT family. This prompted us to use NMR to solve the 3D structures of ZHD from yeast Bcd1p and Hit1p to highlight the structural similarity in the zf–HIT family. We identified structural features associated with the requirement of Hit1p and Bcd1p ZHD for cell growth and box C/D snoRNA stability under heat stress. Altogether, our data suggest an important role of ZHD could be to maintain functional folding to the rest of the protein, especially under heat stress conditions.

Introduction

Zinc-binding proteins are one of the largest protein superfamilies in eukaryotes and represent up to 10% of the human proteome [1]. These proteins contribute to functionally important protein–protein or protein–nucleic acid interactions for regulation of gene expression including transcription regulation, chromatin remodeling, and mRNA stability and processing [2]. The most common types of coordination environment for zinc-finger (ZnF) motifs are the CCCC and CCHH type (C for cysteine and H for histidine), and the classification of the zinc-binding proteins in different subfamilies relies on a combination of these ZnF motifs. In the TRASH (trafficking, resistance, and sensing of heavy metals) superfamily, the members of the zf–HIT family share the zf–HIT domain (ZHD), which is characterized by a fold in "treble-clef" [3,4]. The name of this family derives from the yeast protein Hit1, which is the first protein for which ZHD was defined [5]. The globular 3D fold of the ZHD was described for the first time in the ZNHIT2 protein and consists of two or four β-strands followed by a C-terminal short α-helix packed against the second β-sheet [4]. Amino acid sequence analysis revealed that the zf–HIT family is

divided into three distinct subgroups (Fig. 1). The first subgroup includes proteins with the interleaved CCCC and CCHC ZnF motifs [first zinc finger (ZnF1) and second zinc finger (ZnF2)] that bind two zinc atoms. The CCHC ZnF motif is not conserved in the second and third subgroups, leading to the proposal that these subgroups bind a single zinc ion [4]. This type of classification is also consistent with results of phylogenetic analysis of zf–HIT-containing proteins. Indeed, the first subgroup includes proteins with a single ZHD with two ZnF motifs, whereas the second and third subgroups include a ZHD consisting of a single ZnF motif. The second and third groups are also characterized by the presence of extra domains such as the PAPA-1 homology sequence and the DEAD-box helicase, respectively [4].

ZHD is mainly found in nuclear proteins involved in gene regulation, chromatin remodeling, and pre-snoRNP assembly, but its precise function remains largely unknown. Six Zinc finger HIT domain-containing proteins (ZNHIT1 to 6) are present in the human proteome and three in the yeast *Saccharomyces cerevisiae* proteome (Fig. 1) [6]. In the rest of the paper, mammal proteins are written in uppercase and yeast proteins in lowercase. The ZNHIT1 protein specifically associates with class I histone deacetylase, which was suggested to reduce the acetylation level of histone H4 in the CDK6 promoter region [7]. Moreover, ZNHIT1 protein is associated with helicases TIP49/RuvBL1 and TIP48/RuvBL2 (here called RuvBL1/2) within the complex SRCAP (SNF2-related CBP activator protein; aka hINO80). Its counterpart SWR1 complex (SWR-C) in yeast [8] contains the putative homolog of ZNHIT1 (i.e., the vacuolar protein sorting-associated protein 71, Vps71p, also Swc6p) and proteins Rvb1/2, which are the yeast counterparts of RuvBL1/2. Affinity purification and mass spectrometry (AP-MS) analysis showed that the second protein ZNHIT2 of the human zf–HIT family associates with RuvBL1/2 and RPAP3 (Tah1p in yeast) [9,10]. ZNHIT2 has no known homolog in yeast. The third protein ZNHIT3 (Hit1p in yeast) or human thyroid hormone receptor interacting protein 3 (TRIP3) is a cofactor of the hepatocyte nuclear factor 4α, which is a transcription factor and a member of the steroid hormone receptor superfamily [11]. Mutations in the hepatocyte nuclear factor 4α gene are known to cause maturity-onset diabetes of the young [12]. Recently, ZNHIT3(TRIP3)/Hit1p in human and yeast, respectively, was reported as new cofactor of the platform protein NUFIP1 (Rsa1p in yeast) involved in box C/D small nucleolar ribonucleoprotein (snoRNP) assembly and tightly associated with RuvBL1/2 [13,14]. Like ZNHIT1, the ZNHIT4 (INO80B) protein was reported to be a core component of the INO80 complex, which also includes RuvBL1/2 [15,16]. Recent structural data indicate that the yeast counterpart of ZNHIT4, Ies2p (Ino eighty subunit 2), interacts with proteins Rvb1/2 to recruit these proteins within the INO80 complex [17]. ZNHIT5 (also DDX59 for DEAD box polypeptide 59) protein is a relatively uncharacterized member of the DEAD-box-containing RNA helicase family of proteins that is known to play a critical role in many aspects of RNA metabolism. Finally, the last member of the family, ZNHIT6 (also BCD1 for box C/D snoRNA protein 1), is the ortholog of yeast Bcd1p that was identified by high-throughput genetic screening of yeast mutants associated with defects in non-coding RNA biogenesis [18]. Sequence analysis of the 366 aa of Bcd1p revealed the presence of a ZHD, which is conserved in human and is similar to the one found in the N-terminal part of the TRIP3/Hit1p protein (Fig. 1 and Supplementary Fig. S1). Taken together, these data emphasize the close connection between the zf–HIT proteins and the RuvBL1/2/Rvb1/2 ATPases.

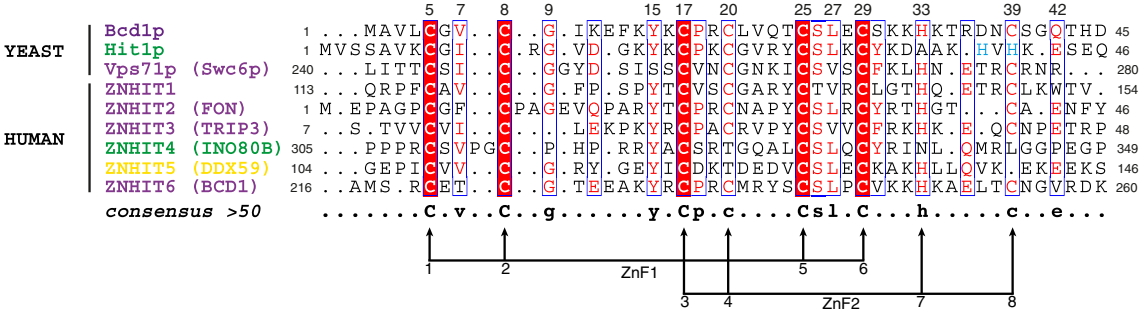

Fig. 1. Sequence comparison between members of the zf–HIT family. Multiple-sequence alignment of different known ZHD sequences obtained from Pfam (Bateman et al., 2004) and made with the ESPript 3.0 program [54] and manually optimized. The cysteine and histidine residues of Bcd1p coordinating zinc ions are indicated by black arrows pointing upwards toward the bottom of the sequences. Numbering at the top corresponds to yeast Bcd1p. Histidine residues involved in the coordination of the second zinc ion in the ZHD of Hit1p are in blue. The three subgroups are in different colors corresponding with the name of the sequences: purple, green, and yellow, for respectively, the first, second, and third subgroups [4].

TIP49(RuvBL1)/Rvb1 and TIP48(RuvBL2)/Rvb2 are two homologous, highly conserved ATP-binding proteins belonging to the AAA+ (ATPases associated with diverse cellular activities) superfamily (for review, see Ref. [19]). They are crucial for a large number of cellular processes and are involved in the assembly of an eclectic set of protein or ribonucleoprotein complexes in the cytoplasm and the nucleus, including various ATP-dependent chromatin remodeling machines such as INO80, SWR1, and p400 [20–24], the histone acetyltransferase TIP60 complex [20], the box H/ACA and box C/D ribonucleoprotein particles [25–27], transcription regulation complexes [28,29], the telomerase complex [30], the RNA polymerase II [31], PIKKs (phosphatidylinositol-3-kinase-like kinases) such as mTOR and SMG1 [32,33], and axonemal dynein [34].

In the recent years, our team has made a particular effort to decipher the mechanisms through which snoRNPs are assembled. Each box C/D snoRNP includes a unique box C/D guide RNA, but they all share a common set of four core proteins, SNU13/Snu13p, NOP58/Nop58p, NOP56/Nop56p, and Fibrillarin/Nop1, in human/yeast, respectively. The box C/D snoRNPs are catalysts for ribose 2′-*O*-methylation during the biosynthesis and processing of the pre-rRNA, and these modifications take place in functional regions such as decoding and peptidyltransferase centers [35]. Concerning the snoRNP biogenesis, the individual depletion of the proteins RuvBL1/Rvb1 and RuvBL2/Rvb2 affects the cellular level of box C/D snoRNAs and leads to incorrect localization of the snoRNP core proteins, both in human and yeast [36,37]. In yeast, the ability of Rvb2 to bind and/or hydrolyze ATP is essential for the accumulation of box C/D snoRNAs [38].

Interestingly, ZNHIT3/Hit1p, which was recently described as a new snoRNP assembly factor specific to the box C/D pathway, is also required for the proper accumulation of box C/D snoRNAs [13,14]. Protein Bcd1 also contributes to the specific stability of the box C/D snoRNAs in *Saccharomyces cerevisiae* and is essential for cellular viability [18,39]. In addition, RNA immunoprecipitation experiments revealed that BCD1 is specifically associated with nucleoplasm precursors of snoRNAs U3 and U8 [40,41]. RNAi-mediated depletion of BCD1 resulted in a significant reduction in the amounts of U3, U8, and U14 but also in a change in the location of U3 snoRNP [40]. These associations probably take place in large assembly complexes, since BCD1 protein is co-purified with proteins NOP58, NOP56, NUFIP1, PIH1D1, and RuvBL1/2 [40]. Pull-down assays using recombinant BCD1 allowed partial mapping of these interactions [40,41]. The truncated 1–360 form of protein BCD1, which contains the ZHD, interacts *in vitro* with Fibrillarin, NUFIP1, and RuvBL1/2, and these interactions are modulated by ATP. The presence of the C-terminal domain of BCD1 is required to establish an association with SNU13. Finally, no direct interaction has been observed with PIH1D1. Recently, BCD1 was shown in close association in cells with RuvBL1/2 in an early protein-only complex of the snoRNP biogenesis pathways [13]. Altogether, these results show that BCD1/Bcd1p is a major factor in the biogenesis of box C/D snoRNP.

Here, we report the results of new functional and structural analysis of the Bcd1 and Hit1 yeast proteins that advance our understanding of the box C/D snoRNP biogenesis pathway. Through domain-mapping experiments, we show that ZHD of Bcd1p (ZHD–Bcd1p) is necessary but not sufficient for its function, even if it is not involved in direct RNA binding. Interestingly, we demonstrate that Bcd1 is however able to nonspecifically bind different RNAs in a size-dependent manner. Our data reveal that zinc coordination is nonetheless crucial for the ability of Bcd1p to maintain the box C/D snoRNAs in steady state. Thus, the mutation of the ZnF2 of Bcd1p exhibits a temperature-sensitive phenotype. Using NMR, we solved the high-resolution structures of the ZHD of both Bcd1p (ZHD–Bcd1p) and Hit1p (ZHD–Hit1p) to highlight the determinants of yeast ZHD proteins involved in the box C/D snoRNP assembly. Our data also demonstrate that these two domains adopt similar folds and that their swap did not alter the function of Bcd1p. All these data are discussed with respect to past classification and genetic evolution of ZHD proteins.

Results

Human and yeast sequence analysis of zf–HIT family

Respectively, three and six members of the zf–HIT family are expressed in the yeast *S. cerevisiae* and in human. Multiple sequence alignment confirmed the conservation of eight residues, including seven cysteines and one histidine, which may coordinate two zinc ions with the following spacing: C_1xxC_2-C_5xxxC_6 interleaved with C_3xxC_4-$H_7xxxxxC_8$ (Fig. 1). The first, second, fifth, and sixth positions correspond to zinc ion ligands in the ZnF1, and the third, fourth, seventh, and eighth positions correspond to the ZnF2. Nevertheless, residues corresponding to the fourth, seventh, and eighth ligand positions are not strictly conserved in Hit1, ZNHIT4, and ZNHIT5 proteins. This observation raised the question of the fold of theZnF2 motif in these proteins.

In addition to the eight zinc-coordinating residues, other amino acids are significantly conserved (consensus line, Fig. 1), for example, a Val or hydrophobic residue in position 7, a Gly residue in position 9, a Tyr residue in position 15, a Ser residue in position

26, a Leu or Val residue in position 27, and a Glu residue in position 42.

Remarkably, two factors involved in the biogenesis of box C/D snoRNP, proteins Hit1 and Bcd1 and their respective counterparts TRIP3 and BCD1 in human, belong to the zf–HIT family. Given our team's interest in the assembly of these particles in yeast, we focused our work on Hit1p and Bcd1p.

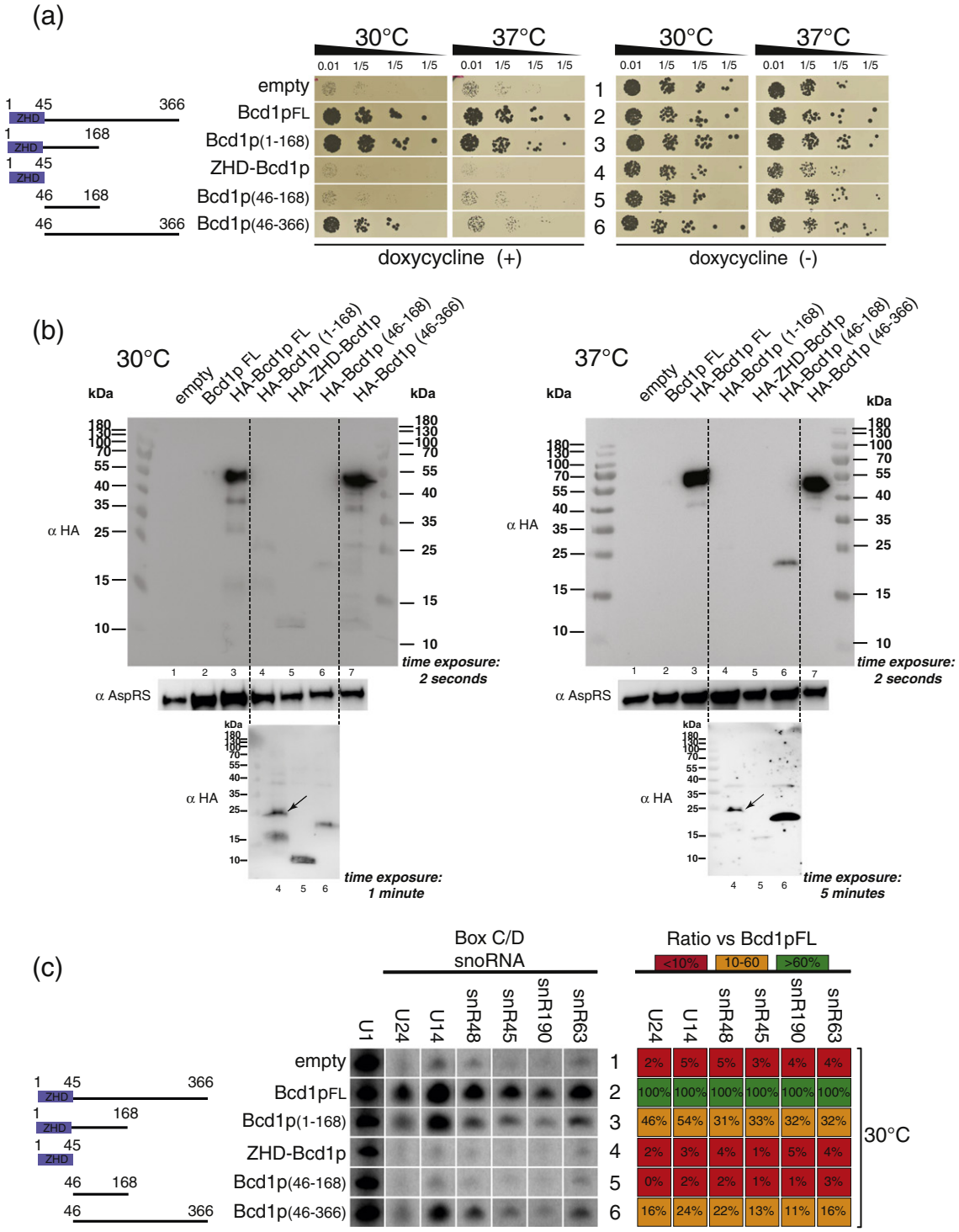

Fig. 2 (*legend on next page*)

The ZHD of Bcd1p is required for the functionality of the protein

Previously, we showed that the Rsa1p-binding domain of Hit1p, but not its ZHD, is required for the function of Hit1p in snoRNP biogenesis [14]. To test the functional importance of the ZHD of Bcd1p in this pathway, we designed several fragments based on sequence conservation and secondary structure prediction (Fig. 2a). First, each fragment was tested in a complementation assay by ectopic expression in the yeast strain *tetO*$_7$::*BCD1* in which expression of the endogenous Bcd1p is repressed upon treatment with doxycycline [18]. The presence of doxycycline (Fig. 2a, left panel *versus* right panel) completely inhibited growth when the cells were transformed with the empty vector p413-TEF (row 1), confirming that Bcd1p expression is essential for cell viability, at both 30 °C and 37 °C. By contrast, the ectopic expression of the full-length 1–366 Bcd1p (row 2) restored growth similar to that in the untreated cells (Fig. 2a, left panel *versus* right panel). Only fragment 1-168 that includes the ZHD allowed complementation at both temperatures (row 3). Even so, the ZHD was not sufficient for complementation (row 4) but was apparently required to maintain the cell viability, since no growth was observed with fragment 46-168 (row 5). This fragment-based approach to complementation assays, which was not previously performed on Bcd1p, revealed that lack of ZHD did not have the same drastic effect since fragment 46-366 allowed partial growth recovery, although only at 30 °C (row 6). The different fragments are not expressed at same levels as shown by western blot analysis of extracts prepared from cells expressing an HA-tagged version of these fragments (Fig. 2b). The amounts of fragments 1-168 (lanes 4) and 46-168 (lanes 6) are similar but much lower (~3-fold change at 30 °C) than the amounts of full-length Bcd1p (Bcd1p-FL) (lanes 3); fragment 46–366 (lanes 7) is expressed even at a higher level (~1.4-fold change at 30 °C). Nevertheless, only expression of fragment 1–168 allowed an apparent growth similar to the one obtained upon expression of Bcd1p-FL. This showed that the first 168 aa of the N-terminal end represent a functional domain *in vivo*. Interestingly, we showed that the ZHD plays an essential role in the function of the protein and consequently in cell viability.

The ZHD of Bcd1p contributes to the steady-state level of the box C/D snoRNAs

Previously, T.R. Hughes' team demonstrated that Bcd1p depletion causes a specific and drastic decrease in the amount of box C/D snoRNAs in the yeast strain *tetO*$_7$::*BCD1* upon doxycycline treatment [18,39]. We next checked for a correlation between the ability of each fragment to complement the growth defect of the *tetO*$_7$::*BCD1* strain and to maintain the amount of box C/D snoRNAs. The steady-state levels of a selected series of box C/D snoRNAs were analyzed by Northern blot hybridization on total RNA extracted from cells expressing the different constructs at 30 °C (Fig. 2c). U1 snRNA was used as negative control and as the internal reference for quantification. The resulting data are in agreement with those obtained in the complementation assays (Fig. 2a). Indeed, the absence of Bcd1p (Fig. 2c, row 1) led to a 25-fold average decrease in the levels of the box C/D snoRNAs, while complementation with Bcd1p-FL restored a high level of these RNAs (row 2). Fragment 1–168 (row 3) and to a lesser extent fragment 46-366 (row 6) restored the level of snoRNAs partially but sufficiently to ensure cell growth. These results

Fig. 2. Functional analysis of Bcd1p domains. (a) Complementation assays. Different fragments of Bcd1p were expressed in *tetO*$_7$::*BCD1* (R1158) strain transformed with the recombinant p413-TEF(*HIS3*) vector. In this strain, expression of the endogenous gene *BCD1* is repressed in the presence of doxycycline [18]. The panel on the left represents the different fragments, and ZHD is identified by a blue rectangle. Transformed cells were harvested from His$^-$ plates, and a stock dilution with A_{600} = 1 per mL was prepared in sterile water. The first sample was diluted to A_{600} 0.01, four successive cascade dilutions with a factor of 1/5 were prepared, and 10 µL of each samples were spotted on solid selective (His$^-$) media prepared in the presence or absence of 50 µg/mL doxycycline. Cell growth was assessed after 72 h at 30 °C and 37 °C. The strain transformed with the empty vector p413TEF was used as a negative control (empty). (b) Western blot analysis of equal amounts of total cell lysates from *tetO*$_7$::*BCD1* (R1158) strain transformed with the recombinant p413-TEF(*HIS3*)-HA, grown at 30 °C and 37 °C and expressing the different HA-tagged fragments. Tagged proteins were detected with anti-HA (α-HA) antibodies. AspRS protein used as loading control was detected using specific anti-AspRS (α-AspRS) antibodies. (c) Northern blot analysis and heat map representation of steady-state levels of six representative box C/D snoRNAs at 30 °C during the exponential growth phase. Total RNAs were extracted from recombinant *tetO*$_7$::*BCD1* (R1158) cells used in the complementation assays, and 10 µg were fractionated on 6% polyacrylamide denaturing gels. After transfer to Zeta-Probe membrane (Biorad), RNAs were detected by hybridization with specific 5′ ^{32}P-radiolabeled oligonucleotides probes (see Materials and Methods) and visualized with a Phosphorimager (Typhoon 9410, GE Healthcare). U1 snoRNA was used as an internal control. The figure was built by cutting the bands obtained at the same exposure from the Northern blot membrane. The radioactivity in each snoRNA band was quantified using ImageQuant software version 5.2 (Molecular Dynamics). The percentage of snoRNA in the different total RNAs extracts was calculated from the radioactivity in each band relative to the radioactivity in the band of U1 snRNA. The percentage of each snoRNA relative to the WT cells is presented on the right.

suggest that the contribution of Bcd1p to the expression of box C/D snoRNAs relies at least in part on its ZHD.

NMR solution structure of the ZHD of Bcd1p

To learn more about the minimal fragment 1-168 of Bcd1p, we sought to produce a recombinant form using a standard immobilized metal ion affinity chromatography (IMAC) approach in *Escherichia coli*. Unfortunately, after several attempts, we were still not able to perform full purification. To go further in our functional analysis of ZHD–Bcd1p, we decided to solve the NMR solution structure of fragments 1–45 of Bcd1p.

We first checked for the presence of zinc ions in ZHD–Bcd1p *in vitro*. Native MS analysis revealed the presence of two zinc ions for a total monoisotopic mass of 5465.39 ± 0.01 Da, which is in agreement with the expected mass (ZHD–Bcd1p −3H +2Zn, 5337.5–3.03 + 130.76 = 5465.23 Da) (Supplementary Fig. S2A). The need for zinc ions for correct folding of ZHD–Bcd1p was then highlighted using a large excess of EDTA that completely deteriorated the $^{1}H–^{15}N$ heteronuclear single quantum coherence (HSQC) NMR spectrum of the protein (Supplementary Fig. S3A).

The use of two temperatures (298 K and 313 K) was required to reach an almost complete NMR assignment. Next, a long range $^{1}H–^{15}N$ HSQC spectrum showed a neutral tautomeric form of the imidazole ring of His33, with the protonation of nitrogen $N^{\delta 1}$ [42]. Thus, inter-proton distance restraints derived from 2D and 3D nuclear Overhauser enhancement spectroscopy (NOESY) spectra, together with zinc-coordination restraints (see Materials and Methods), enabled us to access the solution structure of ZHD–Bcd1p.

The 20 most representative conformers obtained after water refinement with RECOORD scripts are shown in Fig. 3a, and the statistics for the calculation are listed in Table 1. With RMSD values of 0.44 ± 0.06 Å and 1.28 ± 0.13 Å, respectively, for the backbone and heavy atoms of the ordered

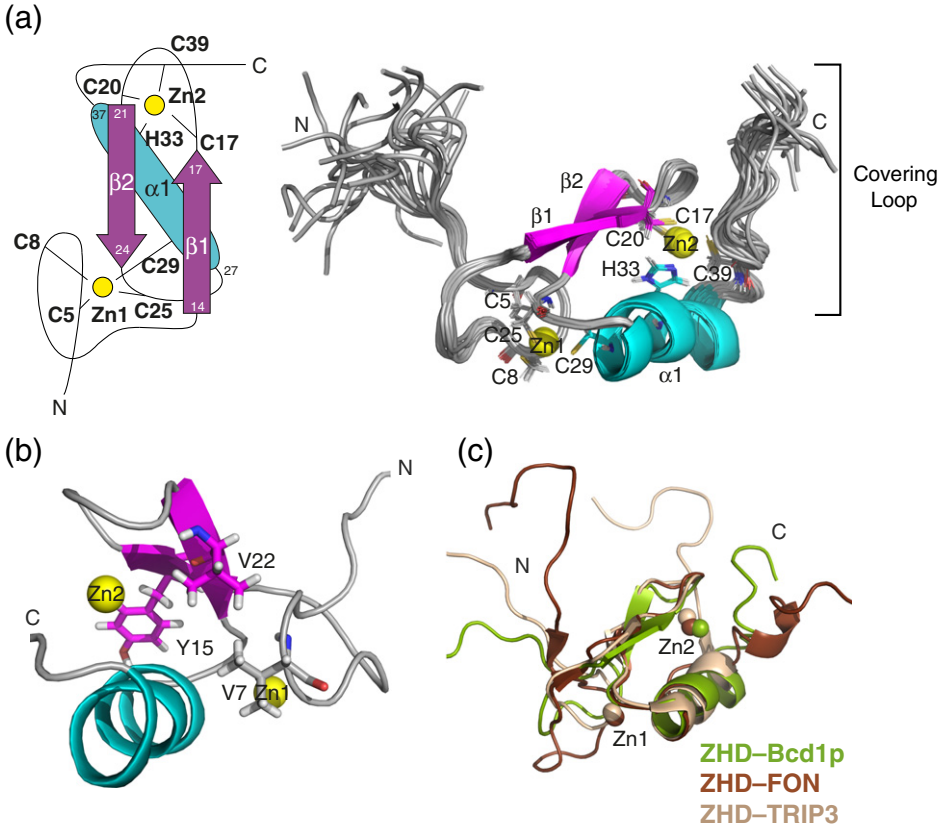

Fig. 3. Solution structures of the ZHD of Bcd1p. (a) Topology diagrams of ZHD–Bcd1p and cartoon representation of the 20 NMR structures with the lowest energies. Zinc ions are in yellow and secondary structures for α-helices in cyan and of β–strands in magenta. Cysteine and histidine residues involved in the zinc coordination are labeled and their side chains are represented by lines. (b) Ribbon representation of the first NMR structure of ZHD–Bcd1p. The side chains of residues Val7, Tyr15, and Val22 are labeled and represented by sticks. (c) Superimposition of the ZHD structures of Bcd1p (1-45) (green), FON (1-46) (brown, PDB code 1X4S), and TRIP3 (7-46) (wheat, PDB code 2YQQ).

Table 1. Statistics of the 20 final solution structures of the Bcd1p and Hit1p ZHDs. The RMSD were calculated using residues 5-39 for ZHD–Bcd1p and 6-41 for ZHD–Hit1p

	ZHD–Bcd1p	ZHD–Hit1p
NMR distances constraints		
Total NOE	902	932
Intra-residue	204	208
Inter-residue		
Sequential (|i - j| = 1)	248	266
Medium-range (|i - j| < 5)	158	156
Long-range (|i - j| > 5)	292	302
Zinc-related restraints	27	26
Dihedral angle restraints	9	10
Average constraints/residues	18.8	19.0
Structure statistics		
Average number of noe violations (>0.5 Å)	0.1 ± 0.3	0.0
Deviations from idealized geometry		
Bond lenght (.10–3 Å)	3.629 ± 0.261	3.604 ± 0.157
Bond angle (°)	0.607 ± 0.031	0.550 ± 0.034
Impropers (°)	1.394 ± 0.173	1.147 ± 0.073
Mean CNS energy (kcal mol^{-1})	−1348.40 ± 47.2	−1502 ± 16.3
Ramachandran plot statistics (%)		
Residues in most favored regions	67.8	68.6
Residues in additional allowed regions	28.9	29.9
Residues in generously allowed regions	2.0	1.2
Residues in disallowed regions	1.3	1.3
Average CNS pairwise RMSD (Å)		
Backbone atoms	0.44 ± 0.06	0.28 ± 0.06
Heavy atoms	1.28 ± 0.13	1.30 ± 0.14

region 5-39, the ensemble of NMR structures is well defined.

In detail, this ZHD comprises successively a structured loop (5–13), a two-stranded antiparallel β-sheet (14–17 and 21–24) and an α-helix (27–37) (Fig. 3a). The first zinc ion is located between the N-terminal structured loop and the very beginning of the α-helix, and its binding site is formed by Cys5, Cys8, Cys25, and Cys29 (Fig. 1). The second zinc ion is located between the loop connecting the two β-strands and the α–helix, and its binding site is formed by Cys17, Cys20, His33, and Cys39 (Fig. 3a). The average distance between the two zinc ions is 12.82 ± 0.08 Å.

We observed that the second zinc ion is protected by a covering loop in the C-terminal part of ZHD–Bcd1p (37-45), creating a more crowded neighborhood for the second ion than for the first (Fig. 3a). The loop is stabilized in part by the side chain of Arg19, which belongs to the connecting loop between the two β-strands. Moreover, the second zinc finger motif clamps the β-sheet over the α-helix and thus could be needed for the stabilization of secondary structures of ZHD–Bcd1p. It contrasts slightly with the first zinc finger motif, which appears more as an appendix positioned at the beginning of the fold (Fig. 3a). However, as expected, the two zinc finger motifs are arranged in a treble-clef-type domain, which is locked by hydrophobic contacts involving residues Val7 and Val22 (Fig. 3b).

Coordination of zinc ions is crucial for the function of the ZHD of Bcd1p in snoRNP biogenesis

With the help of our structural data highlighting the binding mode of zinc ions in ZHD–Bcd1p, we decided to check if the capacity of Bcd1p to coordinate zinc ions contributed to protein functionality. Thus, we introduced several combinations of point mutations in the full-length protein that consisted of the substitution of the first two cysteines of ZnF1 and/or ZnF2 by Serine (Fig. 4a). Each variant was expressed in *E. coli*, purified, and analyzed by circular dichroism to estimate protein secondary structure. All the variants were soluble and stable. Supplementary Fig. S4 showed that both single, mutated proteins ($ZHD_{C5S+C8S}$–Bcd1p and $ZHD_{C17S+C20S}$–Bcd1p) lost typical helical secondary structure, compared to wild-type (WT) Bcd1p, but remained identical to each other. The double-mutated variant ($ZHD_{C5S+C8S+C17S+C20S}$–Bcd1p) showed much less secondary structure than each of the single-mutated variants. In addition, we substituted the solvent-exposed amino acid Tyr15 by alanine (Figs. 1, 3b, and 4a), this residue being conserved in yeast only in ZHD involved in the box C/D snoRNP assembly pathway (i.e., Hit1p and Bcd1p, but not Vps71p).

We then tested the contribution of the substituted residues to cell growth (Fig. 4b) and to the steady-state level of box C/D snoRNAs (Fig. 4c). Complementation of full-length proteins with mutations in

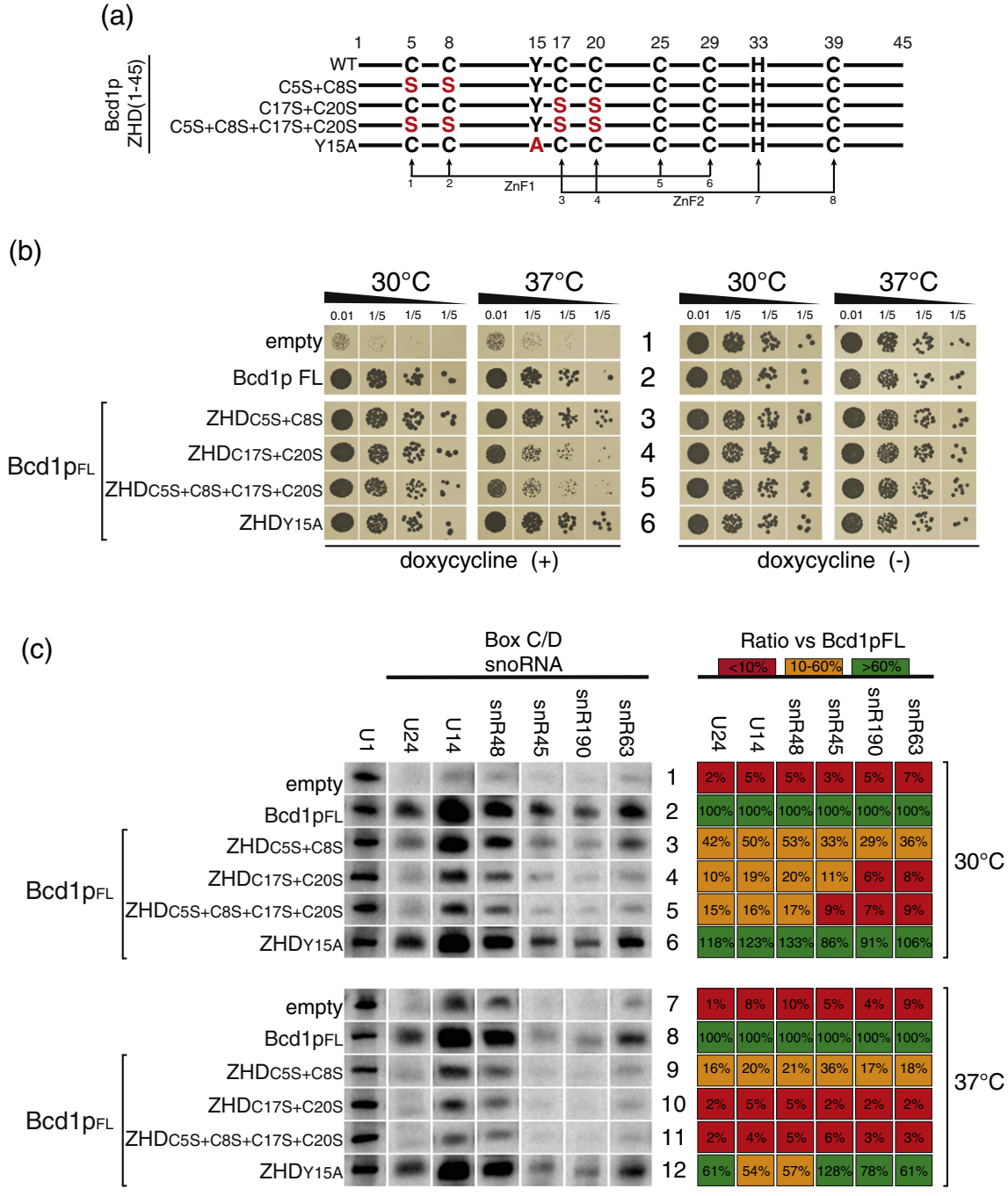

Fig. 4. Functional analysis of the ZHD of Bcd1p in the full-length context. (a) Representation of mutations in ZHD. Cysteine (C) residues substituted by serine (S), and tyrosine (Y) residue substituted by alanine (A) in four variants of Bcd1p-FL. (b) Complementation assays performed as in Fig. 2a for variants of the ZHD. (c) Northern blot analysis of steady-state levels of different box C/D snoRNAs performed as in Fig. 2b.

one of the two zinc fingers allowed growth comparable to that of the WT at 30 °C (rows 3–4) but significantly decreased the amounts of box C/D snoRNAs (rows 3–4). Interestingly, ZnF2 mutations led to a greater reduction in the amount of snoRNA than the ZnF1 mutations, but no cumulative effects were observed either on growth or snoRNA levels, when the two ZnF motifs were mutated (Fig. 4b–c, compare row 3 with rows 4 and 5). Remarkably, in terms of snoRNA amounts, point mutations in ZnF1 and ZnF2 reproduced the behavior of fragments 1–168 and 46–366, respectively (Fig. 2b, rows 3

and 6 *versus* Fig. 4c, rows 3 and 4). More impressively, a growth defect was observed at 37 °C when the ZnF2 was modified, again without a cumulative effect in the double mutants (Fig. 4b, rows 4 and 5). First, we observed a global drop in snoRNA amounts with increasing temperature. Then, the remarkable growth defect in the ZnF2 mutant at 37 °C was even more clearly associated with a drastic reduction in the amounts of snoRNAs (Fig. 4c, row 10). These data clearly reinforce the role played by the ZHD of Bcd1p in snoRNP biogenesis. More precisely, the heat sensitivity induced by mutations in ZnF2 strongly suggests that this motif contributes more significantly to the ZHD function than ZnF1. In agreement with this hypothesis, observation of the 3D structure of ZHD–Bcd1p revealed that the ZnF2 motif was involved in the correct positioning of the secondary structures (Fig. 3a).

Second, we wondered if the part of functionality carried by the ZHD in Bcd1p could be based on interactions with protein partners. Thanks to its conservation and solvent exposure, the Tyr15 residue, which is intrinsically able to establish polar and/or hydrophobic contacts, was a target of choice to address this question (Fig. 3b). However, we observed that the Y15A mutation did not significantly impair growth or snoRNAs amounts whatever the conditions tested (Fig. 4b, row 6, and Fig. 4c rows 6 and 12). A single mutation was probably not sufficient to conclude on the protein binding properties of ZHD–Bcd1p, and we thus leave this question open. Since no clear effect was observed upon mutation of residue with protein-interface properties, we next hypothesized that the ZHD interacts with other entities such as nucleic acids or simply maintains a functional entity of folding for the Bcd1p-FL.

The ZHD of Bcd1p is not a DNA/RNA interaction module

Examination of the electrostatic potential of ZHD–Bcd1p derived from our 3D structure revealed a mainly positive charge distribution (Supplementary Fig. S5A) featuring nucleic acid binding properties shared by numerous zinc finger proteins. To check whether the ZHD of Bcd1p contributed to nucleic acid binding, we used electrophoretic mobility shift assays (EMSA) to assess its ability to bind *in vitro* a 20-mer polydIdC oligonucleotide or a box C/D snoRNA (Fig. 5). Recombinant His-tagged full-length and truncated Bcd1p, that is, ZHD–Bcd1p and fragment 46-366 lacking the ZHD (Bcd1p–ΔZHD), were produced in *E. coli* and purified by IMAC. In addition, the ZHD of Hit1p was tested for the sake of comparison. As shown in Fig. 5a, at the highest concentration (20 μM), the Bcd1p-FL significantly retarded migration of the radiolabeled oligonucleotide dIdC (RNP1). Bcd1p–ΔZHD caused the same band shift as Bcd1p-FL, suggesting that its ZHD is not required for nucleic acid binding. This is in agreement with the fact that neither ZHD–Bcd1p nor ZHD–Hit1p displayed binding properties for the polydIdC oligonucleotide. Interestingly, a 10-fold lower concentration (2 μM) of Bcd1p and Bcd1p–ΔZHD was sufficient to allow complete complex formation with the U14 box C/D snoRNA (RNP2, Fig. 5b).

These data show that Bcd1p exhibits a medium RNA-binding affinity. Furthermore, it appears that the ZHD of Bcd1p, although necessary for cell growth and for maintaining high levels of snoRNAs, is not involved in direct RNA interactions.

Bcd1p interacts nonspecifically with RNAs but binding relies on RNA length

Given the interaction observed *in vitro* between Bcd1p and the U14 snoRNA, we investigated on the specificity of Bcd1p toward this family of RNAs by EMSA. By comparison with U14, we first observed that Bcd1p exhibits a similar affinity for the U3Δ2,3,4 snoRNA, a functional truncated version of U3 previously characterized by our group (Fig. 6a). The U3 snoRNA contains two K-turns that are formed, respectively, by the C′/D motif and by the U3-specific B/C motif. To verify if these K-turn motifs are responsible for the binding of Bcd1p, we used two variants of the U3Δ2,3,4 RNA mutated for the B box (variant U3Δ2,3,4-mutB) or for the D box (variant U3Δ2,3,4-mutD). These mutations are known to abolish the formation of the corresponding K-turns and the recruitment of Snu13p [43]. As shown in the Fig. 6a, the affinity of Bcd1p is similar for the WT and the two U3 RNA variants, suggesting that Bcd1p has no specificity for K-turn-containing RNAs.

Then, we tested its association with various RNAs other than box C/D snoRNAs. For this purpose, we used an approach of competition by EMSA (Fig. 6b). Bcd1p was incubated simultaneously with the radiolabeled U14 snoRNA and with an increasing concentration of unlabeled RNA competitor. The unlabeled U14 snoRNA was used as control competitor. As observed in the Fig. 6b, a concentration of 500 nM of unlabeled U14 is necessary to fully inhibit the association of Bcd1p with the radiolabeled RNA. As other competitors, we used molecules from various RNA families, that is, the SelN mRNA motif that is dedicated to the incorporation of selenocysteine during the translation, yeast tRNAs, the snR36 box H/ACA snoRNA, the U4/U6 snRNA duplex that is a component of the spliceosome, and a fragment of the genomic RNA of the Rous sarcoma virus (RSV). Interestingly, we noticed that the capacity of these molecules to compete with the radiolabeled U14 is proportional to their size. Indeed, the smallest molecules SelN (59 nt) and

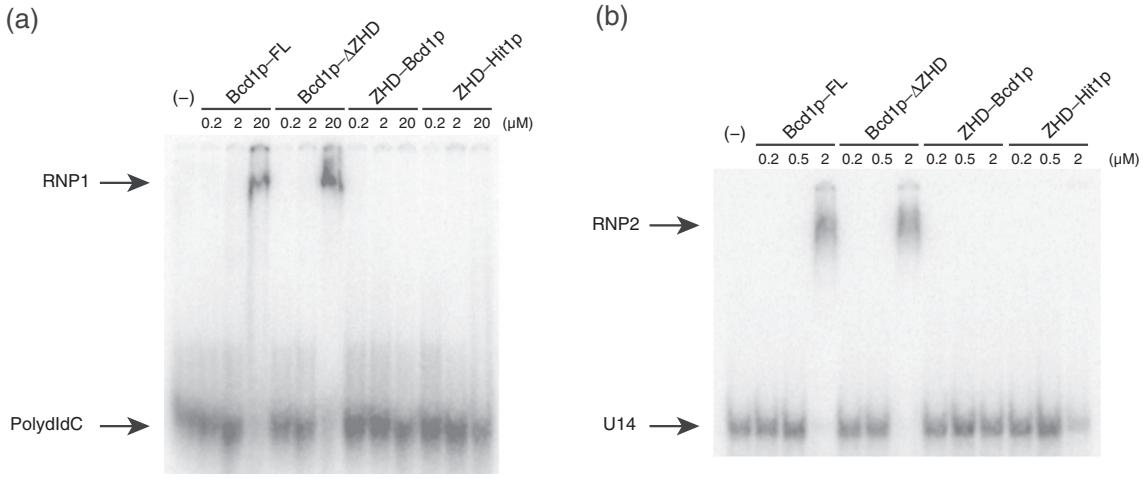

Fig. 5. Bcd1p associates with nucleic acids but has higher affinity for RNA. (a) Bcd1p has very low affinity for a DNA polymer. ^{32}P-labeled 20-mer dIdC oligonucleotide was incubated with increasing amounts (0.2; 2; 20 mM) of Bcd1p-FL, Bcd1p–ΔZHD lacking the ZHD, ZHD–Bcd1p, and ZHD–Hit1p in conditions described in Materials and Methods. The complexes formed were fractionated by EMSA using 8% polyacrylamide native gel. The positions of the Bcd1p:polydIdC (RNP1) complex and the free polydIdC are indicated on the left side of the autoradiogram. (b) Bcd1p affinity for U14 snoRNA. ^{32}P-labeled U14 snoRNA was incubated with increasing amounts (0.2; 0.5; 2 mM) of the proteins used in panel A. The complexes formed were fractionated like in panel A, except that 6% acryl native gel was used. The positions of the Bcd1p:U14 RNA (RNP2) complex and the free U14 RNA (U14) are indicated on the left side of the autoradiogram.

tRNAs (70 nt) do not compete, the snR36 snoRNA (182 nt), which has an intermediate size and is the closest to U14 (128 nt), competes similarly as U14 (Fig. 6b). Finally, the two largest molecules, U4/U6 snRNAs (248 nt) and RSV (266 nt) show the maximal competitor effect, since a concentration of 125 nM is sufficient to prevent the complex formation with radiolabeled RNA.

Collectively, these data show that Bcd1p has RNA-binding capacity, likely by interacting with the phosphate backbone of RNA. It exhibits no apparent sequence specificity, because interaction is driven by the length of the RNA molecule.

The ZHD of Hit1p is functional in Bcd1p

As hypothesized above, we next wondered if the role of ZHD–Bcd1p lies in its ability to maintain functional folding to the rest of the protein. To test this hypothesis, we investigated if the ZHD of Bcd1p could be swapped with another ZHD. Genetic constructs expressing chimeric proteins of Bcd1p encompassing yeast ZHD of Hit1p and Vps71p were generated to perform complementation assays (Fig. 7a). As control, we fused Bcd1p to the C-terminal extremity of the double zinc-finger motif of Rph1p, a protein that does not belong to the zf–HIT family. The ZHDs of Hit1p and Vps71p exhibited the ability to restore the cell growth at 30 °C, while the ZnF–Rph1p did not (Fig. 7b, rows 3 and 4). The amounts of snoRNA obtained upon the expression of the Hit1p chimera were close to those obtained with Bcd1p-FL, except snoRNA snR45 (Fig. 7c, rows 2 and 3). For the Vps71p chimera, the amounts were similar to those obtained with fragment 46–366 of Bcd1p (compare Fig. 2c, row 6 and Fig. 7c, row 4). Surprisingly, the Rph1p chimera, despite expressed at equivalent levels compared to the WT protein (Fig. 7d), displayed an important growth defect at 30 °C associated with very low amounts of snoRNAs. Finally, under heat stress (37 °C), only the Hit1p chimera enabled similar growth to the Bcd1p-FL (Fig. 7b, rows 2 and 3).

The full functionality of ZHD–Hit1p in Bcd1p observed under normal and stress conditions leads us to several conclusions. The presence of yeast ZHDs at the N-terminal part of Bcd1p appears to be required for adequate production of snoRNP for efficient cell growth. However, the presence of zinc ions does not contribute to the functionality of the protein, since the Rph1p chimera is not functionally effective. Moreover, it demonstrates that a swap of the N-terminal zinc finger domain could be more destabilizing for the function of the protein than a deletion. Thus, we can assume that the ZHD maintains functional folding to the entire Bcd1p.

The result obtained under heat stress conditions, which implied efficient production of snoRNP by active assembly factors, reinforces the hypothesis of a crucial role for Bcd1p in this adaptive pathway. This could explain why Vps71p, which has not been shown to be involved in snoRNP biogenesis, does not fully retrieve complementation capacity at 37 °C through its ZHD when it is fused to Bcd1p. These data suggest that only Bcd1p and Hit1p share some

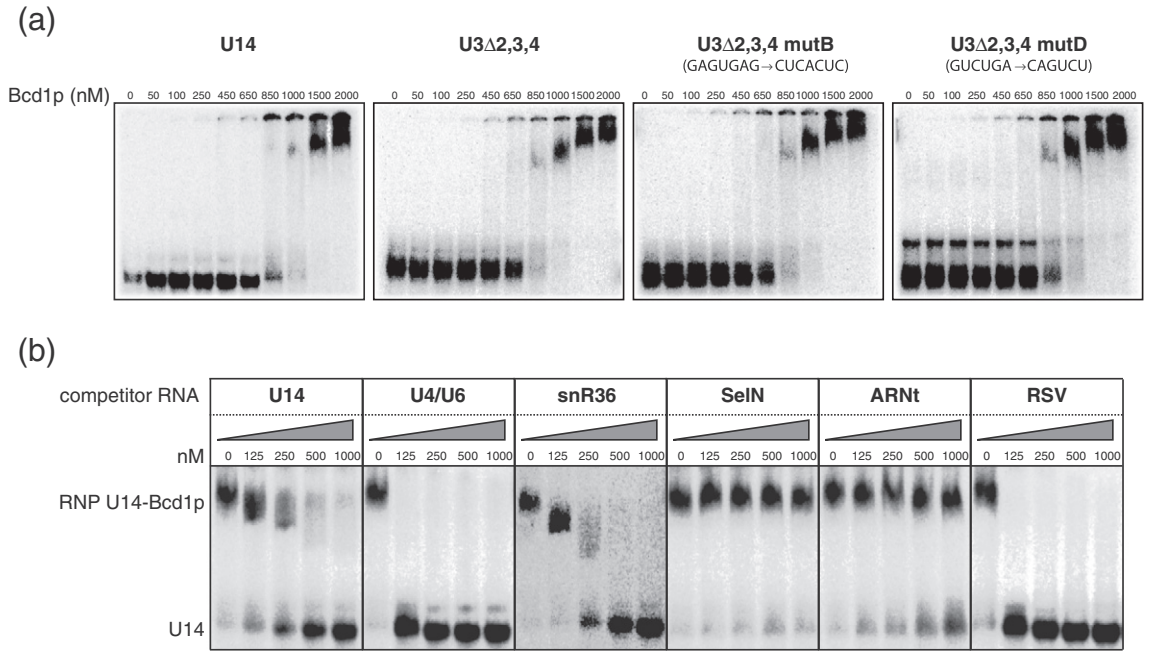

Fig. 6. *In vitro* Bcd1p interacts nonspecifically with RNAs, and affinity relies on the length of the RNA molecule. (a) EMSA between recombinant Bcd1p and radiolabeled U14, U3Δ2,3,4, U3Δ2,3,4 mutB et U3Δ2,3,4 mutD snoRNAs. RNAs were incubated with an increasing range of Bcd1p (from 50 nM to 2 μM). Mutations of B and D boxes totally disrupt the respective B/C and C′/D motifs as previously shown by Ref. [43]. (b) Measurement by EMSA of the affinity of Bcd1p for a set of RNAs of variable length. The affinity of Bcd1p to each RNA was assessed by competition assay between the radiolabeled U14 snoRNA and unlabeled RNA competitors. Recombinant Bcd1p was incubated at a concentration of 1 μM, with 5 fmoles of radiolabeled U14 snoRNA and an increasing concentration of unlabeled RNA (from 125 nM to 1 μM). The unlabeled U14 snoRNA was used as control competitor. The competitors are of different length: SelN mRNA (59 nt), tRNA (70 nt), U14 box C/D snoRNA (128 nt), snR36 box H/ACA snoRNA (182 nt), U4/U6 snRNAs duplex (248 nt), and RSV viral RNA (266 nt corresponding to the fragment 691–956 [55]).

common features of their respective ZHD that appear to be functionally interchangeable.

NMR solution structure of the ZHD of Hit1p

Given the functional redundancy of Bcd1p and Hit1p ZHDs, we decided to solve the solution structure of ZHD–Hit1p (fragment 1-46) to identify shared structural determinants with ZHD–Bcd1p. Until now, Hit1p has been classified as a protein with a single ZnF motif. However, detailed observation of the sequence alignment enabled us to identify not only a potential CCCC zinc finger (Cys8, Cys11, Cys28, and Cys32) but also a hypothetical second zinc coordination motif with a CCHH pattern (Cys20, Cys23, His39, and His41) (Fig. 1). Confirming the presence of these two zinc ions in ZHD–Hit1p will be important because it would be the only member of the zf–HIT superfamily to exhibit a singular narrow HxH motif at the C terminus. First, native MS analysis of ZHD–Hit1p revealed the ability of the protein to bind predominantly two zinc ions (Supplementary Fig. S2B). Second, a ^{15}N-labeled sample of ZHD–Hit1p containing high concentrations of reducing agents (DTT + TCEP) produced a homogeneous and well-dispersed ^{1}H–^{15}N HSQC NMR spectrum, with the expected number of resonances (considering that ZHD–Hit1p is monomeric) (Supplementary Fig. S3B). As before, a large excess of EDTA was responsible for the deterioration of the ^{1}H–^{15}N HSQC spectrum. Taken together, these data showed that ZHD–Hit1p trapped two zinc ions with one CCCC and, certainly, one CCHH motif.

Next, we obtained the almost complete NMR assignment of ZHD–Hit1p, and a long range ^{1}H–^{15}N HSQC spectrum revealed a neutral tautomeric form with protonated nitrogen $N^{\delta 1}$ for His39 and His41. The neutral form determined for the two imidazole rings was in strong agreement with the ability of this domain to bind two zinc ions. Consequently, as for the ZHD–Bcd1p, the NMR solution structure of ZHD–Hit1p was determined using NOE-derived data supplemented with zinc cluster restraints.

The solution structure of the 20 most representative conformers of ZHD–Hit1p obtained after water refinement with RECOORDS scripts are presented in Fig. 8a. The statistics used for the calculation are listed in Table 1. After exclusion of the disordered

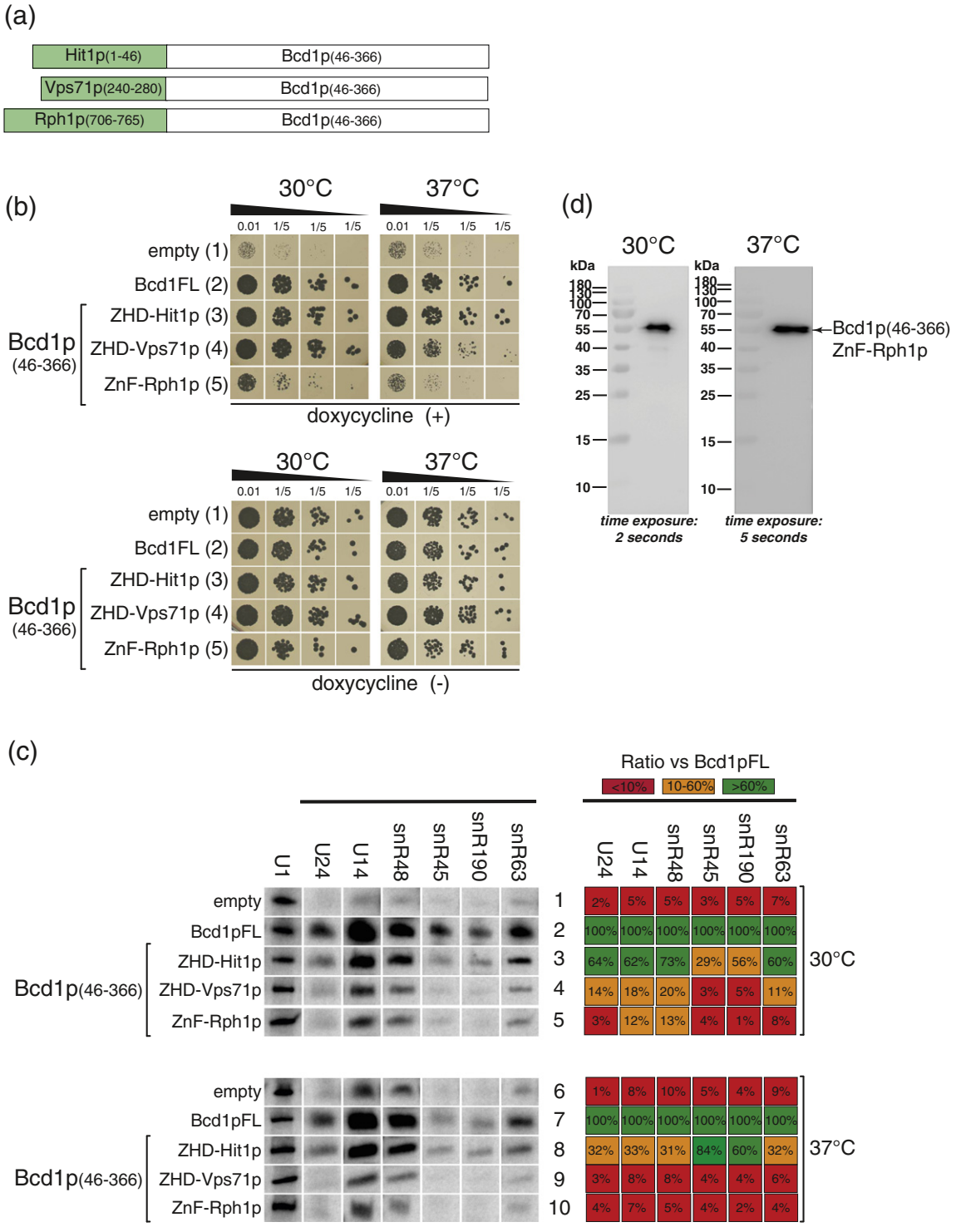

Fig. 7. Functional analysis of chimeric Bcd1p containing different ZnF motifs. (a) Representation of the chimeric proteins for which the endogenous ZHD of Bcd1p was replaced by different yeast ZnF domains (green rectangles): ZHD–Vps71p (residues 240–280) and ZnF–Rph1p (residues 706–765). (b and c) Complementation assays and Northern blot analysis performed as in Fig. 2. (d) Western blot analysis of the amounts of chimeric protein containing the Rph1p ZHD. Detection of a HA-tagged form was performed in conditions described in Fig. 2b.

regions 1–5 and 42–46, we obtained well-converged final ensembles of structures with RMSD values of 0.28 ± 0.06 Å and 1.30 ± 0.14 Å for backbone and heavy atoms, respectively.

In detail, this domain is composed successively of a structured loop (6–16), a two-stranded antiparallel β-sheet (17-20 and 24-27), and a short α-helix (30-33) followed by another structured loop (34–41), which is generated by the presence of the singular HxH motif (Fig. 8a). The first zinc ion is located between the N-terminal structured loop and the α-helix, and its binding site is formed by Cys8, Cys11, Cys28, and Cys32 residues (Figs. 1 and 8a). The second zinc ion is located between the loop connecting the two β-strands and the last structured loop, and its binding site is formed by Cys20, Cys23, His39, and His41 residues (Fig. 8a). The β-sheet packs against the α-helix and the HxH motif to form the second zinc finger. The average distance between the two zinc ions is 12.6 ± 0.1 Å. Like Bcd1p, a treble-clef fold is maintained by hydrophobic contacts involving Ile10 and Val25 residues (Fig. 8b).

Comparison of the Bcd1p and Hit1p ZHD structures

The superimposition of the ZHD–Hit1p structure on that of ZHD–Bcd1p revealed high similarity with the α-helix, with a backbone Cα-RMSD of 0.7 Å between residues 5–30 of Bcd1p and 8–33 of Hit1p (25 residues) (Fig. 8c). The main difference was the singular HxH motif present in Hit1p. This motif prevents the formation of the long helix as in Bcd1p. The fact that these two close histidine residues coordinate a zinc ion creates a sharp rigid turn in the ZHD–Hit1p structure composed of residues Asp35, Ala36, Ala37, and Lys38. However, this difference does not appear to influence the overall folding of these two domains as their 3D structures remain similar and involve similar zinc binding. As evidence, the Zn–Zn distances were very close in the two structures. Supplementary Figure S5B shows a positive electrostatic potential for ZHD–Hit1p with a more pronounced and uniform trend in the N-terminal and central parts than in Bcd1p. However, as in the

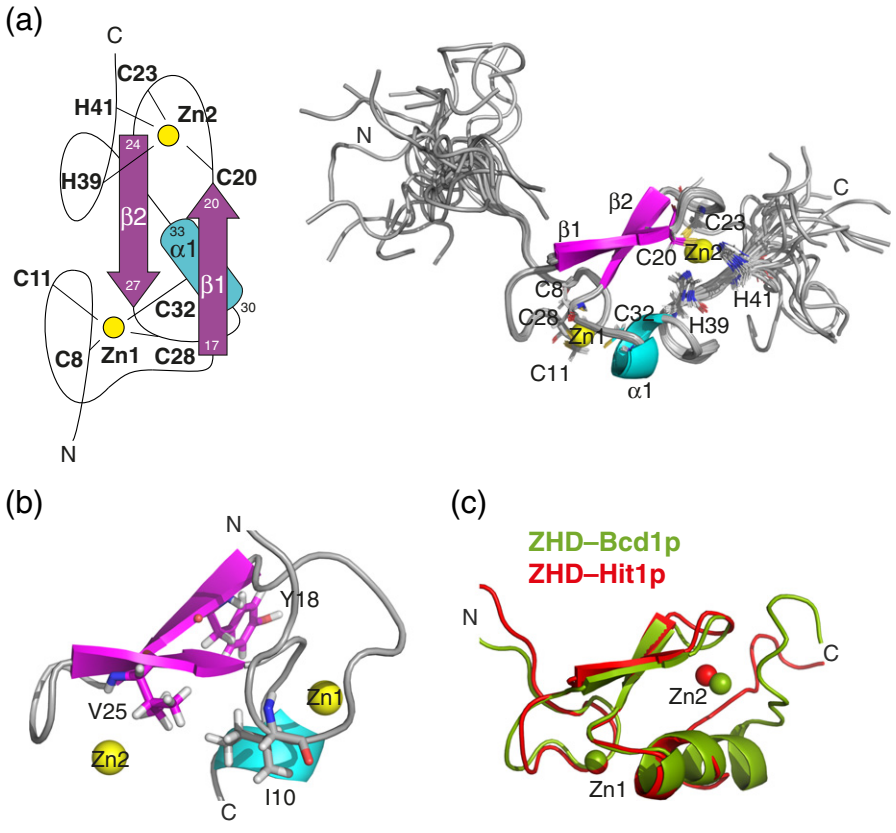

Fig. 8. Solution structures of the ZHD of Hit1p. (a) Topology diagram of ZHD–Hit1p and cartoon representation of the 20 NMR structures with the lowest energies. Zinc ions are in yellow and secondary structures of α-helices in cyan and of β-strands in magenta. Cysteine and histidine residues involved in the zinc coordination are labeled and their side chains are represented by lines. (b) Ribbon representation of the first NMR structure of ZHD–Bcd1p. The side chains of residues Ile10, Tyr18, and Val25 are labeled and represented in sticks. (c) Superimposition of the ZHD structures of Bcd1p (1-45) (green) and Hit1p (1-46) (red).

case of ZHD–Bcd1p, we showed that ZHD–Hit1p was not able to bind nucleic acids (Fig. 5).

Hence, the similar conformation found for ZHD–Hit1p and ZHD–Bcd1p is in good agreement with the results of the domain swapping experiments and confirms the functionality of the chimeric protein ZHD–Hit1p–Bcd1p.

Discussion

Refinement of the organization of the zf–HIT family

As shown in Fig. 3c, the NMR structure of ZHD–Bcd1p is very similar to the two other known structures of the zf–HIT family of the first subgroup, that is, the human proteins ZNHIT2/FON (PDB entry 1X4S) and ZNHIT3/TRIP3 (PDB entry 2YQQ). The protein FON exhibits a 3_{10}-helix, containing the last cysteine of the second zinc-coordinating cluster at the C-terminal position, and a shorter α-helix compared to the one present in Bcd1p. Bcd1p and Hit1p also lack the additional β-sheet present at the N-terminal part of the FON protein. The structure of Bcd1p is more similar to protein FON (Cα-RMSD ~0.8 Å) than to protein TRIP3 (Cα-RMSD ~1.1 Å). Similarly, the ZHD–Hit1p 3D structure is closer to that of FON (Cα-RMSD ~0.7 Å) than to that of TRIP3 (Cα-RMSD ~1.1 Å). Overall, our structural data confirm similar folding in the members of the zf–HIT family.

According to the sequence analysis depicted in Fig. 1, the ZHDs of Bcd1p and Hit1p were predicted to coordinate two and one zinc ions, respectively. He and collaborators thus proposed that Hit1p belongs to the second subgroup whose members bind a single zinc atom (Fig. 1) [4]. Our MS and NMR analyses revealed that ZHD–Hit1p was able to coordinate two zinc ions with the pattern C_1xxC_2-C_5xxxC_6-C_3xxC_4-H_7xH_8. This points to a restrained HxH motif not found in any other members of the zf–HIT family. Finally, we demonstrated experimentally that Hit1p belongs to the first subgroup with Bcd1p and Vps71p.

An exhaustive search of the databases identified the solution structure of a member of the zf–HIT family, ZNHIT5 [or DEAD (Asp-Glu-Ala-Asp) box polypeptide 59]. As suggested by the sequence alignment in Fig. 1, this structure confirms the presence of a single ZnF motif (PDB code: 2YQP). Even in the presence of only one zinc ion, the 3D structure of ZNHIT5 is typical of a ZHD, that is, a treble-clef fold very close to ZHD–Bcd1p (Cα-RMSD ~0.9 Å). However, the missing zinc ion corresponds to the one that, in ZHD–Bcd1, locks the β-sheet against the α-helix (Fig. 3), strongly suggesting that the comparable organization of secondary structures in ZNHIT5 does not depend only on metal coordination. Nonetheless, the close inspection of the 3D structure of ZHD–ZNHIT5 did not reveal any strong stabilizing contacts except one salt bridge between Glu123 and His135. Interestingly, we showed that cysteine to serine substitutions in the ZnF2 motif of ZHD–Bcd1p promoted heat sensitivity in yeast growth correlated with a marked decrease in snoRNA amounts (Figs. 3 and 4). We reasonably link this feature with the destabilization of the tertiary structures. Although we do not know the exact function of ZNHIT5, we can assume that its ZHD contributes to the stability of the protein in the face of heat stress. More importantly, we can hypothesize that coordination of a second zinc ion conveys a functional advantage, in the form of thermal stability, to other members of the zf–HIT family. It is easy to see that whatever the external conditions, a snoRNP assembly factor such as Bcd1p needs to be relatively stable to fulfill its crucial function.

Due to its sequence homology with ZNHIT5, it is very likely that ZNHIT4 has only one ZnF motif too (Fig. 1). In this case, in human, ZNHIT4 and 5 would be the only members of this family with a single zinc finger.

Evolution of Bcd1p and Hit1p zinc fingers

Our past and present analyses in yeast revealed that the two ZHDs do not contribute to the function of Bcd1p and Hit1p in the same way. Indeed, under standard growth conditions, this domain is necessary for the functioning of Bcd1p (Fig. 2) but is not required for the functioning of Hit1p [14]. The sequence comparison between these two proteins and their human counterparts illustrates this difference. The ZHD of Bcd1p showed 90% sequence similarity with that of the human protein BCD1, while the ZHD of Hit1p showed only 30% sequence similarity with that of TRIP3 (Fig. 1). The presence of the same motif in these two proteins involved together in snoRNP biogenesis pathway raises the question of functional redundancy. One possibility is that such redundancy involves lower selection pressure on one of the two ZHD molecules and, hence, divergence for the ZHD sequences of TRIP3/Hit1p.

Moreover, the ZHD sequences of Bcd1p and Hit1p showed 36% similarity, whereas their similarity to the ZHD of Vps71p—the third member of this family in yeast—was only 24% and 10%, respectively. Nonetheless, the data resulting from the functional assays performed with the chimeric proteins showed that among the zf–HIT family, only ZHD–Hit1p can efficiently substitute for the ZHD–Bcd1p in terms of growth and snoRNA amounts (Fig. 7). All these observations, especially the functionality of Hit1p lacking its ZHD at 30 °C [14] and 37 °C (data not shown), corroborate the hypothesis under which TRIP3/Hit1p, although still able to ensure the

functionality of Bcd1p, has started to diverge from other ZHDs.

Hypothesis of a functional link between the members of zf–HIT family and the ATPases TIP49(RuvBL1)/Rvb1–TIP48(RuvBL2)/Rvb2 in human and yeast

In the literature, among the three yeast and the six human proteins of the zf–HIT family, we found a pair of common functional partners, TIP49(RuvBL1)/Rvb1 and TIP48(RuvBL2)/Rvb2 ATPases [6]. These proteins are expressed in different structural forms (monomers, hexamers, and dodecamers) specific to the different multicomponent complexes they compose [44]. This structural diversity confers a specific biological activity to each complex and may reflect the acquisition of novel functions during evolution with the assistance of associated factors such as nucleotides, binding partners, or post-translational modifications. The examples we can cite in the context of this work are Vps71p and ZNHIT4 for the yeast chromatin remodeling complexes SWR-C and INO80-C, respectively, and Bcd1p/Hit1p for the yeast box C/D pre-snoRNPs. One possibility is that the proteins BCD1/Bcd1 and/or TRIP3/Hit1 are able, on one hand, to bind/regulate TIP49/Rvb1 and TIP48/Rvb2 ATPases through their ZHD, and on the other hand, to recruit the platform protein NUFIP1/Rsa1p via the C terminus of TRIP3/Hit1p [14]. Their specific recruitment on the pre-snoRNP to assemble might be enabled by the interaction between NUFIP1/Rsa1p and the core protein SNU13/Snu13p [13,45], which specifically recognizes the snoRNAs through their box C/D motif [46,47]. In this context, the RNA-binding properties of Bcd1p may help to accommodate the complex on the nascent pre-snoRNA once this one has reached a length compatible for binding (Fig. 6).

A functional link between these ATPases and BCD1/Bcd1p can be hypothesized. In yeast, a two-hybrid assay identified an association between Bcd1p and Rvb2, while a direct ATP-dependent interaction has been shown between BCD1 and the TIP49/TIP48 complex [40,41]. One possibility will be to test whether these zinc finger proteins help regulate the biological activity of the TIP49/TIP48 complex and its assembly in different structural forms. The possibility of a direct interaction between ZHDs and the domain II of ATPases could be tested. Indeed, an analysis of dodecameric TIP49/Rvb1 and TIP48/Rvb2 structures indicated that the most likely potential interaction domain is domain II of TIP48/Rvb2. A structural study of domain II of TIP48/Rvb2 interacting with Bcd1p, with or without ATP, would be of interest as knowledge of the structure could explain how the Rvb1/2 proteins are able to re-structure pre-snoRNP and modulate protein–protein interactions within it.

The Bcd1p-FL is required for complete functionality

Throughout our experimental procedure, we mainly focused on the N-terminal part of Bcd1p, that is, its ZHD and fragment 1–168, to demonstrate the functional interest of this region. However, we also demonstrated the importance of having a full-length protein to preserve the same accumulation of snoRNAs as that observed for Bcd1p WT. Since the Bcd1p-FL could be replaced by a Hit1p chimera, we assumed that the ZHD stabilized the functional folding of the entire protein. Interestingly, the secondary structure predictions for Bcd1p-FL emphasize the presence of several β-strands and α-helices for the fragment ΔZHD of Bcd1p, but the overall 3D organization does not match any known or conserved domain, suggesting a new RNA-binding domain (Supplementary Fig. S1). Thus, the ZHD resembles a satellite acting as a fold stabilizer. Nonetheless, we experimentally proved that this unknown fold is able to direct RNA binding. The medium affinity of this binding is in agreement with the role of Bcd1p in the large family of box C/D snoRNAs. In addition, protein partners have already been described in databanks as being associated with Bcd1p using Affinity Capture-RNA, tandem affinity purification, or the two-hybrid assay [48]. Some of these proteins have strong functional links with nucleic acids. We can cite GIS2 and SHE2 gene products, which both bind mRNA; proteins Rtt106 and Ahc2, which are both linked with histone acetylation; MSA2 or MOT3 gene products, which are putative transcriptional factors; and the SFH1 subunit of the chromatin structure-remodeling complex. It would be of great interest to access the 3D structure of Bcd1p full length. This would allow: (i) a better understanding of the role played by its ZHD and (ii) the identification of new surfaces possibly involved in RNA or protein binding.

To go further, Bcd1p is also annotated as a potential partner for proteins of the chaperoning system (Ssa1 to Ssa3, Ssb1, Ssc3, T-complex protein 1 subunit zeta) [48]. We showed that under heat stress, the ZHD of the protein significantly contributes to cell growth. We wonder if this phenotype relies on direct contacts between this domain and proteins of the chaperone family.

Finally, the organization of the mammalian BCD1 diverges significantly from the yeast Bcd1p, whereas similar functions have been described in the two [13,40,41]. It is certain that they share a common ZHD (Fig. 1) but, as often, many sequence insertions are observed in the yeast protein (Supplementary Fig. S1). However, the region downstream from the ZHD is quite nicely conserved, suggesting the ability of the human protein to directly bind snoRNAs through a common 3D fold in the C-terminal domain.

More remarkably, the mammalian Bcd1p counterparts exhibit a supplemental N-terminal region of around 200 residues located upstream from the ZHD and predicted to contain several α-helices. We consequently wonder if this region corresponds to a mammalian gain of function, a hypothesis that remains to be investigated.

Materials and Methods

Plasmid constructs and protein purification

For protein production in *E. coli*, PCR-amplified fragments were cloned between the *Nde*I and *Bam*HI restriction sites of the expression vector pnEA-3CH, leading to the production of fusion proteins with an N-terminal His_6-tag and a PreScission cleavage site (details on the pnEA-3CH on request).

For NMR studies on ZHDs, *E. coli* BL21 (DE3) pRARE2 cells were transformed with pnEA-3CH recombinant plasmids, and uniformly labeled recombinant proteins were produced by growing the cells under agitation in M9 minimal medium containing 1 g/L ^{15}N ammonium chloride (U–^{15}N 98%, Aldrich) and 2 g/L ^{13}C–glucose (U–^{13}C 99%, Isotec), 100 μg/mL ampicillin, 25 μg/mL chloramphenicol, and 100 μM zinc sulfate at 37 °C to an absorbance of 0.6–0.8 at 600 nm (A_{600}), and expression was then induced with 1 mM IPTG for 16 h at 20 °C. The fused proteins were purified using a 5-mL HiTrap TALON column (GE Healthcare) and digested overnight in solution with PreScission Protease at 4 °C to remove the N-terminal His_6-tag. This step was followed by preparative gel filtration (HiLoad 16/60 Superdex 75, GE Healthcare) on an AKTA prime system in 10 mM phosphate buffer (pH 6.4), 150 mM NaCl, and TCEP 0.5 mM. The ZnFs of Bcd1p and Hit1p were concentrated to ~0.8 mM and ~2.2 mM, respectively. For the NMR measurement, 3 mM deuterated DTT and 10% D_2O (vol/vol) were added to the protein samples.

For the production of the proteins used for gel shift assays, *E. coli* BL21 (DE3) pRARE2 cells were transformed and grown under agitation in LB medium containing 100 μg/mL ampicillin and 10 μg/mL chloramphenicol at 37 °C to A_{600} 0.6–0.8, and expression was then induced with 0.3 mM IPTG for 16 h at 20 °C. The fusion proteins were purified using TALON resin (GE Healthcare) and digested overnight in solution with PreScission Protease at 4 °C to remove the N-terminal His_6-tag. This step was followed by preparative size-exclusion chromatography (HiLoad 16/60 Superdex 75, GE Healthcare) on an AKTA prime plus system in 20 mM Hepes-KOH buffer (pH 7.9), 150 mM KCl, and 1.5 mM $MgCl_2$.

For expression in *S. cerevisiae*, Bcd1p and Bcd1p domains (1–45, 1–168, 46–168, and 46–366) were amplified by PCR from *S. cerevisiae* genomic DNA and introduced between the *Bam*HI and *Sal*I restriction sites of the p413TEF (CEN/ARS, *HIS3*) expression vector. Constructs expressing chimeric proteins $Bcd1p_{46–366}$ZHD-Hit1p, $Bcd1p_{46–366}$ZHD-Vps71p, and $Bcd1p_{46–366}$ ZHD-Rph1p were obtained by cloning the ZHD of protein Hit1p, Vps71p, and Rph1p in the recombinant p413TEF::$Bcd1p_{46–366}$. For expression of fragment with an HA tag at their N-terminal ends, *Bam*HI–*Sal*I fragments from the recombinant p413TEF vectors were subcloned into a p413TEF vector containing an HA tag introduced upstream of the *Bam*HI site. The expression level of each HA-tagged fragments was estimated by western blot analysis in previously described conditions using rabbit commercial anti-HA antibodies [14]. Anti-AspRS antibodies were used to detect Asp aminoacyl tRNA synthetase as internal control. *S. cerevisiae* strain *tetO*$_7$::*BCD1* (R1158) [18] was used for the complementation assays.

NMR spectroscopy and resonance assignments

The NMR experiments on $^{13}C/^{15}N$-labeled ZHD–Bcd1p and ZHD–Hit1p samples were performed at 298 K and 313 K on a Bruker Avance III 600MHz spectrometer equipped with a TCI cryoprobe. Spectra were processed with the program TopSpin 3.0 (Bruker) and analyzed with the program Sparky [49]. An almost complete resonance assignment was achieved using combinations of 2D $^1H–^1H$ NOESY, $^1H–^{15}N$ and $^1H–^{13}C$ HSQC spectra, and of 3D HNHA, HNCACB, CBCA(CO)NH, HNCO, H(C)CH–TOCSY, $^1H–^{15}N$ and $^1H–^{13}C$ NOESY-HSQC spectra. All NOESY spectra were recorded with a mixing time of 200 ms. The protonation state of the imidazole rings of histidine residues (and consequently, of which the two nitrogen atoms coordinates zinc ion) was determined using long range $^1H–^{15}N$ HSQC experiments [42].

Calculation of zinc finger structure

The automated procedure of CYANA 3.0 [50] was used to determine the NMR solution structure of each ZHD. Distances between protons were derived from the 2D and 3D NOESY experiments mentioned above. To ensure approximate tetrahedral zinc coordination, we added distance constraints for $Zn–C_\beta$ (3.4–3.6 Å), $Zn–S_\gamma$ (2.2–2.4 Å), $Zn–N_{\varepsilon 2}$ (1.9–2.1 Å), $S_\gamma–S_\gamma$ (3.7–3.95 Å), and $S_\gamma–N_{\varepsilon 2}$ (3.7–3.95 Å) [51]. The final set of restraints resulting from the last CYANA iteration was carefully checked and used for water refinement with RECOORD scripts [52]. Water refinement was also performed in the presence of distance and dihedral constraints around the zinc-coordinating residues. Among the 250 structures calculated, the 20 structures with the lowest overall energy were selected as the most representative. Secondary structures were determined with dss (defines secondary structure), and all figures involving 3D structures were drawn with the program PyMOL [53].

EMSA and competition assays

RNA transcripts were synthesized by *in vitro* transcription with T7 RNA polymerase using a PCR fragment carrying the RNA coding sequence in previously described conditions [45]. The 20-mer dIdC oligodeoxyribonucleotide was purchased from Sigma. The oligodeoxyribonucleotide and the transcribed U14 RNA were 5′ end labeled with T4 polynucleotide kinase in the presence of [γ-^{32}P]ATP and purified with a mini Quick Spin RNA

column (Roche) or by gel electrophoresis. For EMSA, WT or variant Bcd1p and ZHD–Hit1p at different concentrations indicated in figure legends were incubated for 20 min at 4 °C with 5 fmoles of ^{32}P-radiolabeled U14 RNA or polydIdC in buffer D (20 mM Hepes-KOH (pH 7.9), 150 mM KCl, and 1.5 mM $MgCl_2$). The nucleic acid–protein complexes formed were resolved by native gel electrophoresis on 8% and 6% acrylamide gels without EDTA for 20-mer dIdC and U14 RNA, respectively. Bands containing labeled nucleic acids were visualized with a Phosphorimager (Typhoon 9410, GE healthcare). For the competition assays, the protein and the radiolabeled RNA were mixed at the same time with the different concentrations of unlabeled RNA competitors as indicated in figure legends.

Yeast complementation tests

To test whether fragments of Bcd1p can complement depletion of the endogenous Bcd1p protein, we transformed *S. cerevisiae* strain *tetO$_7$::BCD1* (R1158) with recombinant p413 plasmids encoding various WT and mutated fragments of Bcd1p. After transformation, recombinant clones were collected from His$^-$ plates and serial dilutions were prepared in sterile water before spotting on selective His$^-$ plates in the absence or presence of 50 μg/mL doxycycline. Cell growth was assessed after 72 h at 30 °C and 37 °C. Clones of the cells transformed with the empty vector p413TEF were used as negative control.

Measurement of snoRNAs levels in yeast by Northern blot

Total RNAs were extracted from exponentially growing yeast cultures at 30 °C. Northern blot analyses were performed in standard conditions using 10 μg of total RNAs and specific ^{32}P-radiolabeled antisense probes: OG–U1 (5′-GACCAAGGAGTTTGCATCAATGA-3′), OG–snR63 (5′-AAGGTTATGTTGGCCACTCA-3′), OG–snR190 (5′-CGAGGAAAGAAGAGACACCATTATC-3′), OG–snR45 (5′-CCTCAGATCGCTCCGAGA-3′), U14 (5′-TCACTCAGACATCCTAG-3′), OG- snR48 (5′- GAATGGAGAGTACTTAAACTTCACATCC-3′), OG–snR52 (5′-TTCAGAAGGAAGGCAACATAAG-3′), and OG–U24 (5′-GATCTTGGTGATAATTGGTA-3′). Bands containing snoRNAs and U1 snRNA were visualized with a Phosphorimager (Typhoon 9410, GE healthcare). The radioactivity present in each snoRNA and U1 snRNA band was quantified using the ImageQuant software version 5.2 (Molecular Dynamics).

Supplementary data to this article can be found online at http://dx.doi.org/10.1016/j.jmb.2016.04.028.

Accession numbers

Chemical shifts and coordinates of ZHD–Bcd1p and ZHD–Hit1p have been deposited in the Biological Magnetic Resonance Data Bank (http://www.bmrb.wisc.edu/) and in the RCSB Protein Data Bank (http://www.rcsb.org/pdb/home/home.do) under accession numbers 26691/2N94 and 25881/2N95, respectively.

Acknowledgments

This work was supported by the Centre National de la Recherche Scientifique (CNRS), University of Lorraine (UL), the Agence Nationale de la Recherche [ANR-11-BSV8-01503], the PRST IMTS of Plan Etat Région Lorraine, and the Région Alsace for the funding of mass spectrometer. We thank the SCBIM platform of FR3209 CNRS BMCT and UL for NMR facilities. We thank Benjamin Bardiaux for technical support with the ZnF–HIT water-refinement procedure, Alexandre Kriznik for Circular Dichroism technical assistance, and Stéphane Erb for the acquisition of mass spectra.

Received 28 December 2015;
Received in revised form 20 April 2016;
Accepted 23 April 2016
Available online 30 April 2016

Keywords:
zinc finger protein;
Bcd1p;
Hit1p;
box C/D snoRNA;
NMR structure

†B.B. and D.T. contributed equally to this work.

Present address: B. Rothé, Ecole polytechnique fédérale de Lausanne (EPFL) SV ISREC, Station 19, CH-1015 Lausanne, Switzerland.

Present address: J.-M. Saliou, Lille Center for Infection and Immunity, Institut Pasteur de Lille, UMR 8204 CNRS-Université Lille Nord de France, INSERM U1019, 1 rue du Professeur Calmette, 59800 Lille, France.

Abbreviations used:
ZnF, zinc-finger; ZHD, zf–HIT domain; AP-MS, affinity purification and mass spectrometry; TRIP3, thyroid hormone receptor interacting protein 3; snoRNP, small nucleolar ribonucleoprotein; ZnF1, first zinc finger; ZnF2, second zinc finger; HSQC, heteronuclear single quantum coherence; NOESY, nuclear Overhauser enhancement spectroscopy; Bcd1p-FL, full-length Bcd1p; WT, wild-type; RSV, Rous sarcoma virus; SelN, Selenoprotein N.

References

[1] C. Andreini, L. Banci, I. Bertini, A. Rosato, Counting the zinc-proteins encoded in the human genome, J. Proteome Res. 5 (2006) 196–201.
[2] C. Andreini, L. Banci, I. Bertini, A. Rosato, Zinc through the three domains of life, J. Proteome Res. 5 (2006) 3173–3178.
[3] T.J. Ettema, M.A. Huynen, W.M. de Vos, J. van der Oost, TRASH: a novel metal-binding domain predicted to be involved in heavy-metal sensing, trafficking and resistance, Trends Biochem. Sci. 28 (2003) 170–173.

[4] F. He, T. Umehara, K. Tsuda, M. Inoue, T. Kigawa, T. Matsuda, et al., Solution structure of the zinc finger HIT domain in protein FON, Protein Sci. 16 (2007) 1577–1587.
[5] K. Kawakami, B.K. Shafer, D.J. Garfinkel, J.N. Strathern, Y. Nakamura, Ty element-induced temperature-sensitive mutations of *Saccharomyces cerevisiae*, Genetics. 131 (1992) 821–832.
[6] C. Verheggen, B. Pradet-Balade, E. Bertrand, SnoRNPs, ZNHIT proteins and the R2TP pathway, Oncotarget. (2015).
[7] Z. Yang, Y. Cao, X. Zhu, Y. Huang, Y. Ding, X. Liu, Znhit1 causes cell cycle arrest and down-regulates CDK6 expression, Biochem. Biophys. Res. Commun. 386 (2009) 146–152.
[8] A.J. Morrison, X. Shen, Chromatin remodelling beyond transcription: the INO80 and SWR1 complexes, Nat. Rev. Mol. Cell Biol. 10 (2009) 373–384.
[9] C. Jeronimo, D. Forget, A. Bouchard, Q. Li, G. Chua, C. Poitras, et al., Systematic analysis of the protein interaction network for the human transcription machinery reveals the identity of the 7SK capping enzyme, Mol. Cell. 27 (2007) 262–274.
[10] M. Taipale, G. Tucker, J. Peng, I. Krykbaeva, Z.Y. Lin, B. Larsen, et al., A quantitative chaperone interaction network reveals the architecture of cellular protein homeostasis pathways, Cell. 158 (2014) 434–448.
[11] H. Iwahashi, K. Yamagata, I. Yoshiuchi, J. Terasaki, Q. Yang, K. Fukui, et al., Thyroid hormone receptor interacting protein 3 (trip3) is a novel coactivator of hepatocyte nuclear factor-4alpha, Diabetes. 51 (2002) 910–914.
[12] K. Yamagata, H. Furuta, N. Oda, P.J. Kaisaki, S. Menzel, N.J. Cox, et al., Mutations in the hepatocyte nuclear factor-4alpha gene in maturity-onset diabetes of the young (MODY1), Nature. 384 (1996) 458–460.
[13] J. Bizarro, C. Charron, S. Boulon, B. Westman, B. Pradet-Balade, F. Vandermoere, et al., Proteomic and 3D structure analyses highlight the C/D box snoRNP assembly mechanism and its control, J. Cell Biol. 207 (2014) 463–480.
[14] B. Rothe, J.M. Saliou, M. Quinternet, R. Back, D. Tiotiu, C. Jacquemin, et al., Protein Hit1, a novel box C/D snoRNP assembly factor, controls cellular concentration of the scaffolding protein Rsa1 by direct interaction, Nucleic Acids Res. (2014).
[15] L. Chen, Y. Cai, J. Jin, L. Florens, S.K. Swanson, M.P. Washburn, et al., Subunit organization of the human INO80 chromatin remodeling complex: an evolutionarily conserved core complex catalyzes ATP-dependent nucleosome remodeling, J. Biol. Chem. 286 (2011) 11,283–11,289.
[16] J. Jin, Y. Cai, T. Yao, A.J. Gottschalk, L. Florens, S.K. Swanson, et al., A mammalian chromatin remodeling complex with similarities to the yeast INO80 complex, J. Biol. Chem. 280 (2005) 41,207–41,212.
[17] A. Tosi, C. Haas, F. Herzog, A. Gilmozzi, O. Berninghausen, C. Ungewickell, et al., Structure and subunit topology of the INO80 chromatin remodeler and its nucleosome complex, Cell. 154 (2013) 1207–1219.
[18] W.T. Peng, M.D. Robinson, S. Mnaimneh, N.J. Krogan, G. Cagney, Q. Morris, et al., A panoramic view of yeast noncoding RNA processing, Cell. 113 (2003) 919–933.
[19] S. Jha, A. Dutta, RVB1/RVB2: running rings around molecular biology, Mol. Cell. 34 (2009) 521–533.
[20] T. Ikura, V.V. Ogryzko, M. Grigoriev, R. Groisman, J. Wang, M. Horikoshi, et al., Involvement of the TIP60 histone acetylase complex in DNA repair and apoptosis, Cell. 102 (2000) 463–473.
[21] Z.O. Jonsson, S. Jha, J.A. Wohlschlegel, A. Dutta, Rvb1p/Rvb2p recruit Arp5p and assemble a functional Ino80 chromatin remodeling complex, Mol. Cell. 16 (2004) 465–477.
[22] G. Mizuguchi, X. Shen, J. Landry, W.H. Wu, S. Sen, C. Wu, ATP-driven exchange of histone H2AZ variant catalyzed by SWR1 chromatin remodeling complex, Science. 303 (2004) 343–348.
[23] A.V. Samuelson, M. Narita, H.M. Chan, J. Jin, E. de Stanchina, M.E. McCurrach, et al., p400 is required for E1A to promote apoptosis, J. Biol. Chem. 280 (2005) 21,915–21,923.
[24] X. Shen, G. Mizuguchi, A. Hamiche, C. Wu, A chromatin remodelling complex involved in transcription and DNA processing, Nature. 406 (2000) 541–544.
[25] Y. Kakihara, W.A. Houry, The R2TP complex: discovery and functions, Biochim. Biophys. Acta. 2012 (1823) 101–107.
[26] R. Machado-Pinilla, D. Liger, N. Leulliot, U.T. Meier, Mechanism of the AAA+ ATPases pontin and reptin in the biogenesis of H/ACA RNPs, RNA. 18 (2012) 1833–1845.
[27] D.R. Newman, J.F. Kuhn, G.M. Shanab, E.S. Maxwell, Box C/D snoRNA-associated proteins: two pairs of evolutionarily ancient proteins and possible links to replication and transcription, RNA. 6 (2000) 861–879.
[28] Z.O. Jonsson, S.K. Dhar, G.J. Narlikar, R. Auty, N. Wagle, D. Pellman, et al., Rvb1p and Rvb2p are essential components of a chromatin remodeling complex that regulates transcription of over 5% of yeast genes, J. Biol. Chem. 276 (2001) 16,279–16,288.
[29] H. Ohdate, C.R. Lim, T. Kokubo, K. Matsubara, Y. Kimata, K. Kohno, Impairment of the DNA binding activity of the TATA-binding protein renders the transcriptional function of Rvb2p/Tih2p, the yeast RuvB-like protein, essential for cell growth, J. Biol. Chem. 278 (2003) 14,647–14,656.
[30] A.S. Venteicher, Z. Meng, P.J. Mason, T.D. Veenstra, S.E. Artandi, Identification of ATPases pontin and reptin as telomerase components essential for holoenzyme assembly, Cell. 132 (2008) 945–957.
[31] S. Boulon, B. Pradet-Balade, C. Verheggen, D. Molle, S. Boireau, M. Georgieva, et al., HSP90 and its R2TP/Prefoldin-like cochaperone are involved in the cytoplasmic assembly of RNA polymerase II, Mol. Cell, 39 (2010) 912–924.
[32] Z. Horejsi, H. Takai, C.A. Adelman, S.J. Collis, H. Flynn, S. Maslen, et al., CK2 phospho-dependent binding of R2TP complex to TEL2 is essential for mTOR and SMG1 stability, Mol. Cell, 39 (2010) 839–850.
[33] H. Takai, Y. Xie, T. de Lange, N.P. Pavletich, Tel2 structure and function in the Hsp90-dependent maturation of mTOR and ATR complexes, Genes Dev. 24 (2010) 2019–2030.
[34] H. Omran, D. Kobayashi, H. Olbrich, T. Tsukahara, N.T. Loges, H. Hagiwara, et al., Ktu/PF13 is required for cytoplasmic pre-assembly of axonemal dyneins, Nature. 456 (2008) 611–616.
[35] W.A. Decatur, M.J. Fournier, rRNA modifications and ribosome function, Trends Biochem. Sci. 27 (2002) 344–351.
[36] N.J. Watkins, I. Lemm, D. Ingelfinger, C. Schneider, M. Hossbach, H. Urlaub, et al., Assembly and maturation of the U3 snoRNP in the nucleoplasm in a large dynamic multiprotein complex, Mol. Cell. 16 (2004) 789–798.
[37] R. Zhao, Y. Kakihara, A. Gribun, J. Huen, G. Yang, M. Khanna, et al., Molecular chaperone Hsp90 stabilizes Pih1/Nop17 to maintain R2TP complex activity that regulates snoRNA accumulation, J. Cell Biol. 180 (2008) 563–578.

[38] T.H. King, W.A. Decatur, E. Bertrand, E.S. Maxwell, M.J. Fournier, A well-connected and conserved nucleoplasmic helicase is required for production of box C/D and H/ACA snoRNAs and localization of snoRNP proteins, Mol. Cell. Biol. 21 (2001) 7731–7746.
[39] S.L. Hiley, T. Babak, T.R. Hughes, Global analysis of yeast RNA processing identifies new targets of RNase III and uncovers a link between tRNA 5′ end processing and tRNA splicing, Nucleic Acids Res. 33 (2005) 3048–3056.
[40] K.S. McKeegan, C.M. Debieux, S. Boulon, E. Bertrand, N.J. Watkins, A dynamic scaffold of pre-snoRNP factors facilitates human box C/D snoRNP assembly, Mol. Cell. Biol. 27 (2007) 6782–6793.
[41] K.S. McKeegan, C.M. Debieux, N.J. Watkins, Evidence that the AAA+ proteins TIP48 and TIP49 bridge interactions between 15.5K and the related NOP56 and NOP58 proteins during box C/D snoRNP biogenesis, Mol. Cell. Biol. 29 (2009) 4971–4981.
[42] J.G. Pelton, D.A. Torchia, N.D. Meadow, S. Roseman, Tautomeric states of the active-site histidines of phosphorylated and unphosphorylated IIIGlc, a signal-transducing protein from *Escherichia coli*, using two-dimensional heteronuclear NMR techniques, Protein Sci. 2 (1993) 543–558.
[43] N. Marmier-Gourrier, A. Clery, V. Senty-Segault, B. Charpentier, F. Schlotter, F. Leclerc, et al., A structural, phylogenetic, and functional study of 15.5-kD/Snu13 protein binding on U3 small nucleolar RNA, RNA. 9 (2003) 821–838.
[44] K.L. Cheung, J. Huen, W.A. Houry, J. Ortega, Comparison of the multiple oligomeric structures observed for the Rvb1 and Rvb2 proteins, Biochem. Cell Biol. 88 (2010) 77–88.
[45] B. Rothe, R. Back, M. Quinternet, J. Bizarro, M.C. Robert, M. Blaud, et al., Characterization of the interaction between protein Snu13p/15.5K and the Rsa1p/NUFIP factor and demonstration of its functional importance for snoRNP assembly, Nucleic Acids Res. 42 (2014) 2015–2036.
[46] I. Vidovic, S. Nottrott, K. Hartmuth, R. Luhrmann, R. Ficner, Crystal structure of the spliceosomal 15.5kD protein bound to a U4 snRNA fragment, Mol. Cell. 6 (2000) 1331–1342.
[47] N.J. Watkins, V. Segault, B. Charpentier, S. Nottrott, P. Fabrizio, A. Bachi, et al., A common core RNP structure shared between the small nucleoar box C/D RNPs and the spliceosomal U4 snRNP, Cell. 103 (2000) 457–466.
[48] C. UniProt, UniProt: a hub for protein information, Nucleic Acids Res. 43 (2015) D204–D212.
[49] T.D. Goddard, D.G. Kneller, in: University of California SF (Ed.), Sparky 3, 2002.
[50] P. Guntert, Automated NMR structure calculation with CYANA, Methods Mol. Biol. 278 (2004) 353–378.
[51] B. Wang, S.L. Alam, H.H. Meyer, M. Payne, T.L. Stemmler, D.R. Davis, et al., Structure and ubiquitin interactions of the conserved zinc finger domain of Npl4, J. Biol. Chem. 278 (2003) 20,225–20,234.
[52] A.J. Nederveen, J.F. Doreleijers, W. Vranken, Z. Miller, C.A. Spronk, S.B. Nabuurs, et al., RECOORD: a recalculated coordinate database of 500+ proteins from the PDB using restraints from the BioMagResBank, Proteins. 59 (2005) 662–672.
[53] W.L. DeLano, The PyMOL Molecular Graphics System, Version 1.3r1. The PyMOL Molecular Graphics System, Version 13r1, Schrödinger, LLC, New York, 2010.
[54] X. Robert, P. Gouet, Deciphering key features in protein structures with the new ENDscript server, Nucleic Acids Res. 42 (2014) W320–W324.
[55] A. Bar, V. Marchand, G. Khoury, N. Dreumont, A. Mougin, N. Robas, et al., Structural and functional analysis of the Rous sarcoma virus negative regulator of splicing and demonstration of its activation by the 9G8 SR protein, Nucleic Acids Res. 39 (2011) 3388–3403.